Opto-Electronic Engineering

Article

2017, Vol 44, Issue 2

Field-level characterization of strong coupling between excitons and surface plasmon polaritons in J-aggregate/metal hybrid nanostructures

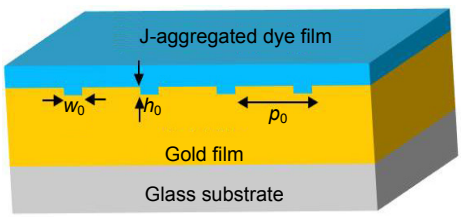

Wei Wang[1,4]*, Ephraim Sommer[2], Antonietta De Sio[2], Parinda Vasa[3], Juemin Yi[2] and Hong Zhang[1,4]*

[1]College of Physical Science and Technology, Sichuan University, Chengdu 610064, China; [2]Institut für Physik, Carl von Ossietzky Universität, Oldenburg 26111, Germany; [3]Department of Physics, Indian Institute of Technology, Bombay 400076, India; [4]Key Laboratory of High Energy Density Physics and Technology of Ministry of Education, Sichuan University, Chengdu 610065, China

Abstract: White-light broadband chirp-compensated spectral interferometry is applied to fully probe the optical response of strongly coupled excitons (Xs) and surface plasmon polaritons (SPPs) in J-aggregate/metal hybrid nanostructures at field level. Under impulsive excitation, amplitude and spectral phase of the sample reflectivity are measured with high precision and the time structure of the electric field emitted by the hybrid modes of the nanostructures is accurately reconstructed. Quantitative description of strong X-SPP coupling is precisely obtained by fitting both measured spectra and phases simultaneously to a Fano lineshape model.

Keywords: surface plasmon polaritons; spectral interferometry; subwavelength nanostructures; strong coupling

DOI: 10.3969/j.issn.1003-501X.2017.02.009 **Citation:** *Opto-Elec Eng*, 2017, **44**(2): 202−208

1 Introduction

Metallic nanostructures can support the strongly confined interface waves: surface plasmon polaritons (SPPs) [1-4]. SPPs have recently been used in a variety of applications due to their ability to guide light on the scale of nanometer. Whereas, intrinsic weak optical nonlinearities and short propagation lengths of SPPs [5] hinder their applications in novel active plasmonic devices. One promising solution is to couple SPPs to nonlinear optical resonances, such as excitons (Xs) in molecular or semiconducting nanostructures. This approach has been widely used in various active plasmonic devices, such as all-optical [6-10] and plasmonic switches [11-15] single-photon transistors [16-17]. Consequently, hybrid nanostructures containing J-aggregate molecules and metallic nanostructures have attracted considerable interest [1, 9, 18-24]. In these systems, vacuum field fluctuations lead to a coherent exchange of energy between ensembles of excitons and plasmons and the formation of new hybrid polariton states. Strong coupling between Xs and SPPs enables an efficient transfer of the strong optical nonlinearities of the excitonic emitters to the passive plasmonic nanostructures on the ultrashort time scale of femtosecond [10, 25-27]. Their relevant coherent control applications and ultrafast nano-plasmonic signal processing are expected to rely on accurate manipulation of the mutual light- matter interactions and accessible control over the resulting polaritonic responses. Therefore, precise characterization of the optical response of the hybrid nanostructures is required and of key importance for designing functional devices with desired tunablility.

In this paper, we demonstrate a field-level characterization of the optical response of J-aggregate/metal hybrid nanostructures by white-light broadband chirp-compensated spectral interferometry [26, 28-32]. We show that both the amplitude and spectral phase of the strongly coupled X-SPP system can be measured with high precision by compensating the chirp in both arms of the in-

Received 13 November 2016; accepted 02 January 2017
* E-mail: w.wang@scu.edu.cn, hongzhang@scu.edu.cn

terferometer. By fitting the measured amplitudes and spectral phases simultaneously to a Fano lineshape model, we can obtain a quantitative description of both the excitonic resonance and the hybrid X-SPP polariton response. We find that the resonance of the majority of J-aggregated molecules, which are not coupled to SPPs, is homogeneously broadened. We also demonstrate accurate reconstruction of the time structure of the electric field emitted by the hybrid nanostructures, corresponding to polarization oscillations with short damping time less than 100 fs.

2 Sample fabrication

The investigated J-aggregate/metal hybrid nanostructure, as schematically shown in Fig. 1(a), consists of a gold nanogroove array coated with a 50-nm-thick J-aggregate dye film. The nanogroove array used in our experiment is fabricated on 500 nm thick gold films, which is evaporated on the surface of a thin chrome layer (5 nm) deposited on top of a 1 mm thick glass plate. The chrome is used for fixing the gold on the glass substrate during cleaning in an ultrasonic bath. Nano-groove arrays with different periods and depths are written by focused ion beam (FIB) milling (FEI: Quanta3d). By using an ion current of 100 nA at a voltage of 30 kV, we are able to prepare high-quality nanogroove arrays with the size of 150 μm×150 μm. Here we show in Fig. 1(b) the SEM picture of the investigated nanogroove array with a period of 430 nm. For the J-aggregated material, we use cyanine dye2, 2-dimethyl-8-phenyl-5,6,5, 6-dibenzothiacarbocyanine chloride(Hayashibara Biochemicals Laboratories, Inc.) dissolved in polyvinyl alcohol (PVA), methanol and water. The procedure is as follows: first, PVA is dissolved in water by sonication for 5 minutes. Then, we add methanol and sonicate for 1 minute. Finally, the dye powder is added and the solution is sonicated for other 5 minutes. A typical concentration of 0.5 moles per dm^3 (5.48 mg dye, 26 mg PVA, 4 ml methanol, 1 ml water) of the J-aggregate in dry PVA is achieved. The groove period is chosen such that the first order polymer/metal plasmon mode is resonant with the J-aggregate exciton at 1.79 eV[25-26]. The hybrid structure exhibits large coupling energy as a result of the high J-aggregate excitonic oscillator strength and the strong local SPP field enhancement near the grooves.

3 Experimental method: spectral interferometry

To fully characterize the complex sample response, high-resolution, angle-resolved spectral interferometry (SI) is introduced to measure both the reflectivity spectra

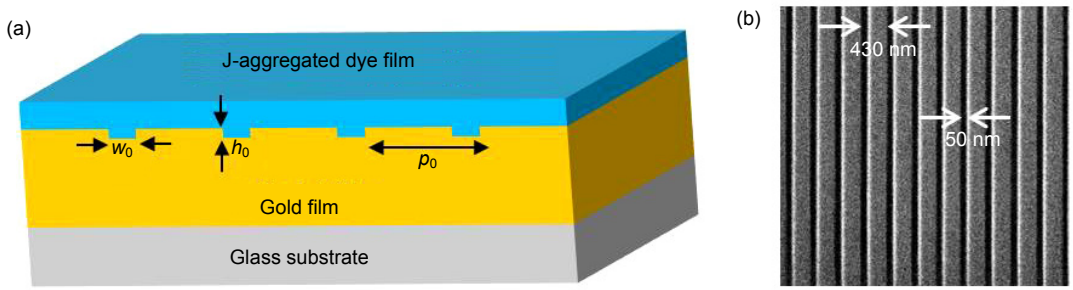

Fig. 1 (a) Schematic of the hybrid nanostructure consisting of a gold nanogroove array with groove period p_0=430 nm, depth h_0=25 nm and width w_0=50 nm, coated with a 50-nm-thick J-aggregate dye film. (b) SEM picture of the uncoated groove array written on a gold film by focus ion beam (FIB).

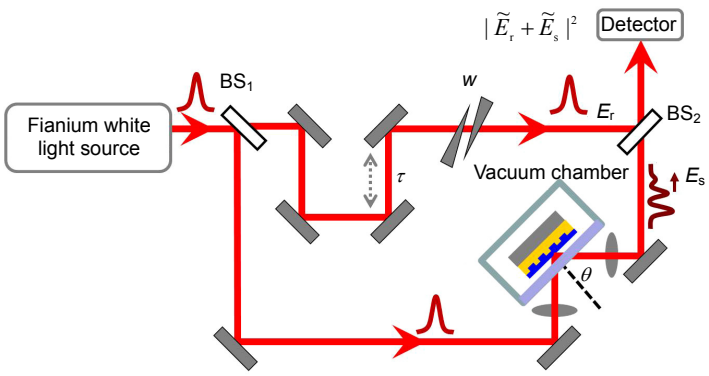

Fig. 2 Angle-resolved spectral interferometry setup (BS: beam splitter, τ: variable delay, w: wedge pair).

$R_0(\omega)$ and the spectral phase $\varphi(\omega)$. The SI measurements are based on a Mach-Zehnder interferometer, as schematically shown in Fig. 2.

Broadband laser pulses generated from an ultrafast coherent white-light source (Fianium SC-450-4) with 80 MHz-repetition rate are split by the first beam splitter (BS_1) and sent through the two arms of a Mach-Zehnder interferometer. One beam with inserted sample in reflection geometry is modulated by its complex response function, resulting in the electric field $E_s(\omega)$. In our experiments, the hybrid nanostructure is isolated in a vacuum chamber to prevent photo-bleaching of J-aggregated dyes. The other beam with electric field $E_r(\omega)$ is the undisturbed reference beam delayed by τ with respect to the sample arm. The two beams are then combined after the second beam splitter (BS_2) and sent to the detector where the interfering field intensity $|E_r(\omega)+E_s(\omega)|^2$ is recorded. Then, the complex sample response, i.e., the reflection coefficient can be obtained:

$$r(\omega)=\sqrt{R_0(\omega)}\exp(\mathrm{i}\varphi(\omega))=\frac{E_s(\omega)}{E_r(\omega)}, \tag{1}$$

Here, $R_0(\omega)$ can be obtained by blocking the reference beam $E_r(\omega)$. $\varphi(\omega)$ can be extracted by identifying the fringe minima and maxima from the interferogram, which is governed by:

$$|E_s(\omega)+E_r(\omega)\mathrm{e}^{-\mathrm{i}\omega t}|^2=(1+|r(\omega)|^2)|E_r(\omega)|^2+ 2|E_r(\omega)|\cdot|E_s(\omega)|\cos(\omega t+\varphi(\omega)). \tag{2}$$

It is noted that the phase extraction becomes challenging in our case due to the presence of additional optical components in the sample arm, such as, front window of the vacuum chamber, focusing and collimating lenses. This material dispersion introduces an unwanted phase shift, which reduces the sensitivity of the extracting the phase contributed only from the hybrid system. To avoid the unwanted phase shift, chirp compensation is performed by introducing one pair of wedges with the same material as those of the additional optical components in the reference arm.

4 Results and discussion

With chirp-compensated Mach-Zehnder interferometer, we first characterized the optical response of J-aggregate dye at field level by performing angle-resolved reflectivity measurements on bare J-aggregate dye coated on a planar gold film. The measurement of the dye absorption in reflection on gold is equivalent to a double-pass transmission experiment through the dye film. All reflectivity spectra are measured at room temperature. The resonance position of the J-aggregate (693 nm, 1.789 eV) is only slightly changing at low temperature (77 K or 10 K)[33].

To obtain the normalized reflectivity spectra, the spectra directly reflected from the gold film are needed. Therefore, we remove one part of the bare dye coating from the sample. The sample is then mounted in the cryostat, where a vacuum environment is provided to prevent the photo-bleaching of the J-aggregates. We first record three sets of data for each incidence of angle on the coated gold film: (i) the fringes (interferogram) due to the interference between the sample and reference arm, (ii) the spectrum of the reflected sample beam by blocking the reference arm and (iii) the spectrum of the reflected reference beam by blocking the sample arm. Then we move the cryostat such that the beam hits on the uncoated region. By repeating the above procedure (i)~(iii), other three sets of data are recorded. Then, we move to the next angle of incidence and repeat the above procedure. The measured reflectivity spectra $R_x(\omega, \theta)$ of the J-aggregate dye coated on gold film as a function of incidence angle are shown in Fig. 3(a).

The spectra are normalized to the reflectivity of the planar gold film. We can clearly see that the spectra are dominated by an angle-independent line originated from the bare dye absorption around 1.8 eV. From the interferograms we can also extract the corresponding angle-resolved spectral phase $\varphi_x(\omega, \theta)$, as shown in Fig. 3(c). With the measured spectra and phase, the complex reflectivity coefficient of the sample can be characterized as:

$$r_x(\omega,\theta)=A_x\exp(\mathrm{i}\varphi_x(\omega,\theta))= \sqrt{R_x(\omega,\theta)}\exp(\mathrm{i}\varphi_x(\omega,\theta)). \tag{3}$$

Where the amplitude of the complex reflectivity coefficient is given as $A_x=\sqrt{R_x(\omega,\theta)}$.

To fully describe the measured optical response of the J-aggregate dye, a Lorentzian oscillator model in the framework of transfer matrix is introduced to reproduce the complex reflectivity coefficient r_x by fitting both R_x and φ_x simultaneously to a sum of Lorentzian oscillator response functions in the framework of transfer matrix. The simulation shows that the J-aggregate dye resonances can be well described by assuming a sum of pure Lorentzian functions for the susceptibility of the bare dye as the following expression:

$$\chi_{\mathrm{dye}}(\omega)=\sum_m\left(\frac{A_m\mathrm{e}^{-\mathrm{i}\phi_m}}{\omega-\omega_m+\mathrm{i}\gamma_m}+\frac{A_m\mathrm{e}^{-\mathrm{i}\phi_m}}{\omega+\omega_m+\mathrm{i}\gamma_m}\right). \tag{4}$$

Here, two Lorentzian oscillators are introduced, corresponding to the indices m=1, 2 representing the main resonance and the additional broad resonance at higher energy, respectively. A_m, ϕ_m and ω_m denote the amplitude, phase and resonance frequency of the individual resonances, respectively. As the J-aggregate dye is dissolved in PVA solution, the dielectric function of the dye film can be written as

$$\varepsilon_1(\omega)=1+f\cdot\chi_{\mathrm{dye}}(\omega)+(1-f)\cdot\chi_{\mathrm{PVA}}. \tag{5}$$

Here, χ_{PVA} represents the susceptibility of the PVA solution which is considered as a constant of 1.4. We also estimate a volume filling factor of the dye f=0.1 in PVA solution. Then the refractive index of the J-aggregate dye

is given as $n_1 = \sqrt{\varepsilon_1}$. Finally, the total complex, reflectivity coefficient can be modeled as $r_x = r_{\text{dye}} / r_{\text{gold}}$, which is related to the complex reflectivity coefficient of dye film r_{dye} and gold substrate r_{gold} respectively. By fitting the measured reflectivity spectra and spectral phase simultaneously to the total complex reflectivity coefficient, a quantitative description of the bare dye resonance can be obtained with high precision. The fitted angle-dependent reflectivity spectra and spectral phase are plotted in Figs. 3(b) and 3(d), respectively. For reference, we also show the measured and fitted spectrum and phase at the incidence angle of 21° in Fig. 3(e). To evaluate inhomogeneous broadening, we plot the spectral response in the complex plane, as shown in Fig. 3(f). In such a representation, the spectrum of a single, purely homogeneously broadened Lorentzian resonance is located on a nearly perfectly circular trace, provided that the susceptibility of the dye film is much less than unity. This is in contrast to an inhomogeneously broadened system, where it would be represented by a severely flattened, elliptical shape[34]. Evidently, the experimental data closely follow a circular trace and show a very good match with the simulated data given by solid line in Fig. 3(f). We conclude that the main resonance of the J-aggregate film is adequately described by a single Lorentzian line shape, suggesting that in the present samples inhomogeneous broadening is apparently weak.

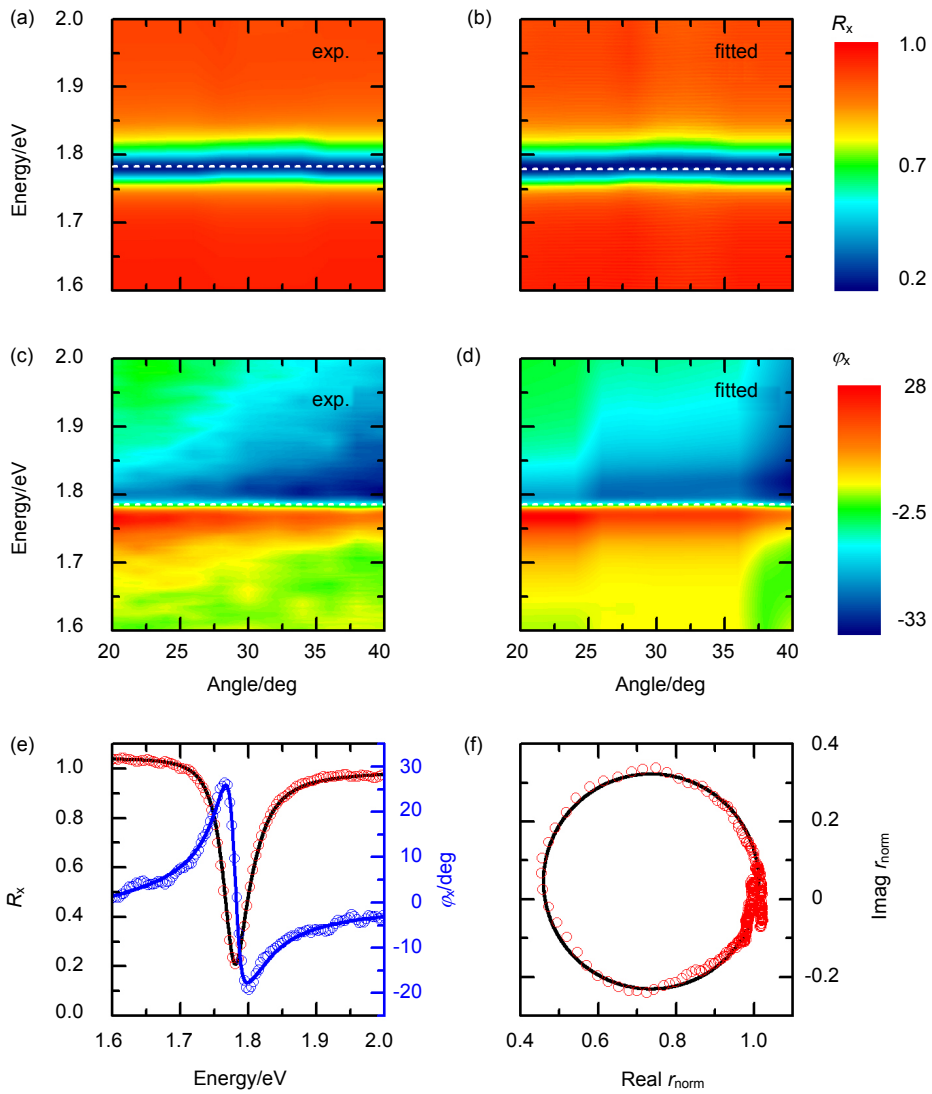

Fig. 3 Angle-resolved reflectivity spectra $R_x(\omega,\theta)$. (a, b) and spectral phase $\varphi_x(\omega,\theta)$. (c, d) of J-aggregate dye coated on planar gold film obtained from SI measurement (a, c) and the fitting (b, d) to Lorentzian oscillator model. The dashed lines mark the dye absorption at around 1.8 eV in (a, b) and the corresponding phase jump in (c, d). (e) Observed (red circles) and fitted (solid black) reflectivity spectra $R_x(\omega)$, and the corresponding observed (blue circles) and fitted (solid blue) spectral phase $\varphi_x(\omega)$, measured at the incidence angle of 21°. (f) The corresponding observed normalized reflection coefficient plotted in complex plane (red circles). The solid black curve is the result fitted to a circular function.

Then, we performed SI measurements on the hybrid J-aggregate/metal nanostructure to characterize the linear optical response of the hybrid system. The measured angle-dependent reflectivity amplitude $R_0(\omega, \theta)$ and phase spectra $\varphi(\omega, \theta)$ are shown in Figs. 4(a) and 4(c).

In Fig. 4(a), a typical anticrossing behavior of the X and SPP resonances can be clearly seen and this indicates a strong X-SPP coupling, resulting in the formation of two hybrid polariton modes: an upper polariton (UP) with higher energy and a lower polariton (LP) with lower energy. As a result, the coupled system shows a normal mode splitting of the UP and LP resonances of $2\hbar\Omega_R$, where Ω_R denotes the Rabi frequency of the system. It is also noted that a prominent absorption band occurs at J-aggregate exciton resonance around 1.79 eV. This is due to the fact that the main enhanced SPP field is localized to small volumes near the grooves. Therefore, a significant portion of the uniformly distributed molecules remains uncoupled due to the sharp variation of SPP field strength in space. J-aggregated molecules located in these regions can strongly couple to the SPP fields. Excitons outside these regions may not or only weakly couple to the SPP field.

With the measured spectra and spectral phase shown in Figs. 4(a) and 4(c), we can readily obtain the complex reflectivity coefficient of the coupled system by following the formula given by equation (1). In such nanogroove arrays, both the narrow X and SPP resonance interfere with a broadband reflection from the gold interface, resulting in typical Fano-like line shapes. Phenomenologically, we can describe the optical response of the coupled system by fitting a sum of oscillator response functions to $R_0(\omega)$ and $\varphi(\omega)$ according to:

$$\sqrt{R_0(\omega)}\mathrm{e}^{\mathrm{i}\varphi(\omega)} = \alpha + \mathrm{i}\beta\sum_m\left(\frac{|\mu_m|^2\mathrm{e}^{-\mathrm{i}\varphi_m}}{\omega-\omega_m+\mathrm{i}\gamma_m}+\frac{|\mu_m|^2\mathrm{e}^{\mathrm{i}\varphi_m}}{\omega+\omega_m+\mathrm{i}\gamma_m}\right). \quad (6)$$

Here, α and β are real-valued slowly varying back ground and scaling amplitudes, respectively. The indices m=1~4 represent LP, UP, the uncoupled J-aggregate resonance, and an additional broad shoulder at ~2 eV attributed to higher vibrionic states or some residual dye monomer. μ_m, φ_m and ω_m denote the effective dipole moment, phase, and resonance frequency of the individual resonances, respectively.

The fitted angle-resolved reflectivity and spectral phase are shown in Figs. 4(b) and 4(d), respectively, which are in good agreement with the experimental data. The amplitude and phase-resolved data allow us to directly extract the relevant parameters for all four resonances with high precision. We compare the measured data with the fitted results in Fig. 5 (a) for angle of incidence of 31°

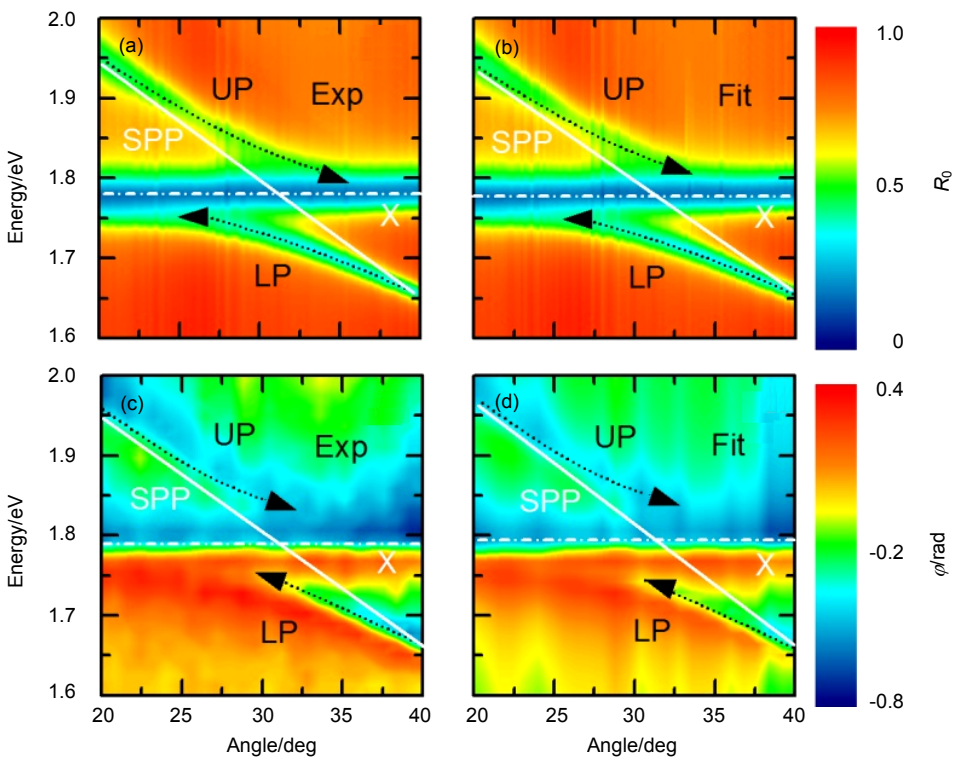

Fig.4 Observed (a) and modeled (b) angle-resolved reflectivity spectra, $R_0(\omega, \theta)$ and corresponding observed (c) and modeled (d) spectral phase, $\varphi(\omega, \theta)$. The black (white) lines mark the coupled (uncoupled) mode dispersions.

around the detuning. We note that both the amplitude and phase spectra are quantitatively reproduced by the Lorentzian oscillator model. This suggests that a possible inhomogeneous broadening of the ensemble of coupled polariton modes has only a minor influence on their optical spectra.

According to equation (6), we can extract the polariton response and deduce the time structure of there-emitted polariton field under weak impulsive excitation. The corresponding electric field amplitudes in the time domain can be written as:

$$E_{\mathrm{r}} = \frac{1}{2\pi}\int_{-\infty}^{+\infty}\widetilde{E}_{\mathrm{r}}(\omega)\exp(-\mathrm{i}\omega t)\mathrm{d}\omega, \tag{7}$$

and

$$E_{\mathrm{s}} = \frac{1}{2\pi}\int_{-\infty}^{+\infty}\widetilde{r}(\omega)\widetilde{E}_{\mathrm{r}}(\omega)\exp(-\mathrm{i}\omega t)\mathrm{d}\omega = \int_{-\infty}^{+\infty}\widetilde{r}(t')\widetilde{E}_{\mathrm{r}}(t-t')\mathrm{d}t'. \tag{8}$$

Then, the response of the system to a fictitious δ-pulse excitation, $E_{\mathrm{r}}(t)=\delta(t)$ is given by the Fourier transform $r(t)=\frac{1}{2\pi}\int_{-\infty}^{+\infty}\widetilde{r}(\omega)\exp(-\mathrm{i}\omega t)\mathrm{d}\omega$. Therefore, measuring $\widetilde{r}(\omega)$ allows us to deduce the time structure of the total electric field emitted by the sample under a δ-pulse excitation. As shown in Fig. 5(a), the experimental spectra can be convincingly described by a sum of Lorentzian response functions, equation (6). Since both amplitude and phase of the phase function have been measured experimentally, this allows us to extract the response of the UP and LP polariton modes by subtracting the response of all other contributions to the reflectivity.

In Fig. 5(b), we show the deduced polariton field for the angle of incidence of θ=31°, where we can see that the field shows polarization oscillations with a beat frequency ω_{UP}-ω_{LP} within the short damping time of <100 fs. The variation of this beat frequency with angle shows a clear anticrossing, the signature of X-SPP Rabi oscillations in the spectral domain.

5 Conclusions

In summary, we use chirp-compensated Mach-Zehnder interferometer to fully characterize the response function of the J-aggregate/metal hybrid structure. Chirp compensation in both arms of the interferometer enables us to measure both the amplitude and spectral phase of the strongly coupled X-SPP system with high precision. Moreover, a Fano lineshape model is used to simultaneously fit the measured amplitudes and spectral phase to obtain a quantitative description of both the excitonic resonance and the hybrid X-SPP polariton response. We find that the bare J-aggregated dye resonance is homogeneously broadened. Also, we reconstruct the time structure of the electric field emitted by the hybrid nanostructures, corresponding to polarization oscillations with short damping time less than 100 fs. We expect that, with properly-designed setup, the chirp-compensated spectral interferometer can be extended to the field-level measurements for other functional nanoplasmonic structures.

Acknowledgements

We thank National Natural Science Foundation of China (61675139, 11374217, 11474210, 11474207); Natural Science Foundation of Chongqing, China (CSTC2014jcyjA 40045).

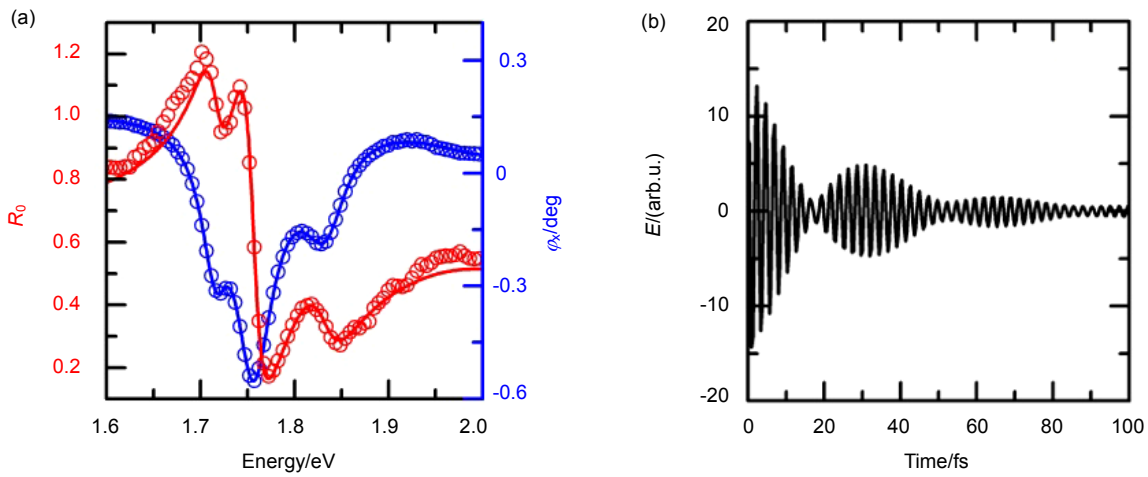

Fig. 5 (a) Experimental (circles) and simulated (solid lines) reflectivity spectra and spectral phases at θ=31°. (b) Time structure of the electric field emitted by the hybrid UP and LP modes at θ=31°, showing distinct polarization beats with frequency ω_{UP}-ω_{LP}.

References

1 Guebrou S A, Symonds C, Homeyer E, *et al*. Coherent Emission from a Disordered Organic Semiconductor Induced by Strong Coupling with Surface Plasmons[J]. *Physical Review Letters*, 2012, **108**(6): 066401.

2 Bozhevolnyi S I, Volkov V S, Devaux E, *et al*. Channel plasmon subwavelength waveguide components including interferometers and ring resonators[J]. *Nature*, 2006, **440**(7083): 508–511.

3 Lal S, Link S, Halas N J. Nano-optics from sensing to waveguiding[J]. *Nature Photonics*, 2007, **1**(11): 641–648.

4 Maier S A, Kik P G, Atwater H A, *et al*. Local detection of electromagnetic energy transport below the diffraction limit in metal nanoparticle plasmon waveguides[J]. *Nature Materials*, 2003, **2**(4): 229–232.

5 Stockman M I. Nanoplasmonics: past, present, and glimpse into future[J]. *Optics Express*, 2011, **19**(22): 22029–22106.

6 Abb M, Albella P, Aizpurua J, *et al*. All-optical control of a single plasmonic nanoantenna-ITO hybrid[J]. *Nano Letters*, 2011, **11**(6): 2457–2463.

7 Dintinger J, Robel I, Kamat P V, *et al*. Terahertz all-optical molecule-plasmon modulation[J]. *Advanced Materials*, 2006, **18**(13): 1645–1648.

8 MacDonald K F, Sámson Z L, Stockman M I, *et al*. Ultrafast active plasmonics[J]. *Nature Photonics*, 2009, **3**(1): 55–58.

9 Schwartz T, Hutchison J A, Genet C, *et al*. Reversible switching of ultrastrong light-molecule coupling[J]. *Physical Review Letters*, 2011, **106**(19): 196405.

10 Vasa P, Pomraenke R, Cirmi G, *et al*. Ultrafast manipulation of strong coupling in metal-molecular aggregate hybrid nanostructures[J]. *Acs Nano*, 2010, **4**(12): 7559–7565.

11 Argyropoulos C, Chen P Y, Monticone F, *et al*. Nonlinear Plasmonic cloaks to realize giant all-optical scattering switching[J]. *Physical Review Letters*, 2012, **108**(26): 263905.

12 Lu H, Liu X M, Wang L R, *et al*. Ultrafast all-optical switching in nanoplasmonic waveguide with Kerr nonlinear resonator[J]. *Optics Express*, 2011, **19**(4): 2910–2915.

13 Pacifici D, Lezec H J, Atwater H A. All-optical modulation by plasmonic excitation of CdSe quantum dots[J]. *Nature Photonics*, 2007, **1**(7): 402–406.

14 Pala R A, Shimizu K T, Melosh N A, *et al*. A nonvolatile plasmonic switch employing photochromic molecules[J]. *Nano Letters*, 2008, **8**(5): 1506–1510.

15 Valev V K, Baumberg J J, Sibilia C, *et al*. Chirality and chiroptical effects in plasmonic nanostructures: fundamentals, recent progress, and outlook[J]. *Advanced Materials*, 2013, **25**(18): 2517–2534.

16 Chang D E, Sørensen A S, Demler E A, *et al*. A single-photon transistor using nanoscale surface plasmons[J]. *Nature Physics*, 2007, **3**(11): 807–812.

17 Hwang J, Pototschnig M, Lettow R, *et al*. A single-molecule optical transistor[J]. *Nature*, 2009, **460**(7251): 76–80.

18 Bellessa J, Bonnand C, Plenet J C, *et al*. Strong coupling between surface plasmons and excitons in an organic semiconductor[J]. *Physical Review Letters*, 2004, **93**(3): 036404.

19 Symonds C, Bonnand C, Plenet J C, *et al*. Particularities of surface plasmon-exciton strong coupling with large Rabi splitting[J]. *New Journal of Physics*, 2008, **10**(6): 065017.

20 Hakala T K, Toppari J J, Kuzyk A, *et al*. Vacuum rabi splitting and strong-coupling dynamics for surface-plasmon polaritons and rhodamine 6G molecules[J]. *Physical Review Letters*, 2009, **103**(5): 053602.

21 Fofang N T, Grady N K, Fan Z Y, *et al*. Plexciton Dynamics: Exciton-plasmon coupling in a J-aggregate-Au nanoshell complex provides a mechanism for nonllinearity[J]. *Nano Letters*, 2011, **11**(4): 1556–1560.

22 Zengin G, Johansson G, Johansson P, *et al*. Approaching the strong coupling limit in single plasmonic nanorods interacting with J-aggregates[J]. *Scientific Reports*, 2013, **3**: 3074.

23 Schlather A E, Large N, Urban A S, *et al*. Near-field mediated plexcitonic coupling and giant rabi splitting in individual metallic dimers[J]. *Nano Letters*, 2013, **13**(7): 3281–3286.

24 Balci S, Kocabas C. Ultra hybrid plasmonics: strong coupling of plexcitons with plasmon polaritons[J]. *Optics Letters*, 2015, **40**(14): 3424–3427.

25 Vasa P, Wang W, Pomraenke R, *et al*. Real-time observation of ultrafast Rabi oscillations between excitons and plasmons in metal nanostructures with J-aggregates[J]. *Nature Photonics*, 2013, **7**(2): 128–132.

26 Wang W, Vasa P, Pomraenke R, *et al*. Interplay between strong coupling and radiative damping of excitons and surface plasmon polaritons in hybrid nanostructures[J]. *ACS Nano*, 2014, **8**(1): 1056–1064.

27 Vasa P, Wang W, Pomraenke R, *et al*. Optical stark effects in J-aggregate-metal hybrid nanostructures exhibiting a strong exciton-surface-plasmon-polariton interaction[J]. *Physical Review Letters*, 2015, **114**(3): 036802.

28 Reynaud F, Salin F, Barthelemy A. Measurement of phase shifts introduced by nonlinear optical phenomena on subpicosecond pulses[J]. *Optics Letters*, 1989, **14**(5): 275–277.

29 Lepetit L, Chériaux G, Joffre M. Linear techniques of phase measurement by femtosecond spectral interferometry for applications in spectroscopy[J]. *Journal of the Optical Society of America B*, 1995, **12**(12): 2467–2474.

30 Ropers C, Park D J, Stibenz G, *et al*. Femtosecond light transmission and subradiant damping in plasmonic crystals[J]. *Physical Review Letters*, 2005, **94**(11): 113901.

31 Rewitz C, Keitzl T, Tuchscherer P, *et al*. Ultrafast plasmon propagation in nanowires characterized by far-field spectral interferometry[J]. *Nano Letters*, 2012, **12**(1): 45–49.

32 Rajendran S K, Wang W, Brida D, *et al*. Direct evidence of Rabi oscillations and antiresonance in a strongly coupled organic microcavity[J]. *Physical Review B*, 2015, **91**(20): 201305.

33 Ceccarelli S, Wenus J, Skolnick M S, *et al*. Temperature dependent polariton emission from strongly coupled organic semiconductor microcavities[J]. *Superlattices and Microstructures*, 2007, **41**(5–6): 289–292.

34 Jurna M, Garbacik E T, Korterik J P, *et al*. Visualizing resonances in the complex plane with vibrational phase contrast coherent anti-stokes raman scattering[J]. *Analytical Chemistry*, 2010, **82**(18): 7656–7659.